# Real-time dynamics in the one-dimensional Hubbard model

Luis Seabra,[1] Fabian H. L. Essler,[2] Frank Pollmann,[3] Imke Schneider,[2] and Thomas Veness[2]
[1]*Department of Physics, Technion - Israel Institute of Technology, Haifa 32000, Israel*
[2]*The Rudolf Peierls Centre for Theoretical Physics, Oxford University, Oxford OX1 3NP, United Kingdom*
[3]*Max-Planck-Institut für Physik komplexer Systeme, Nöthnitzer Straße 38, 01187 Dresden, Germany*
(Received 19 October 2014; revised manuscript received 27 November 2014; published 16 December 2014)

We consider single-particle properties in the one-dimensional repulsive Hubbard model at commensurate fillings in the metallic phase. We determine the real-time evolution of the retarded Green's function by matrix-product state methods. We find that at sufficiently late times the numerical results are in good agreement with predictions of nonlinear Luttinger liquid theory. We argue that combining the two methods provides a way of determining the single-particle spectral function with very high frequency resolution.

DOI: 10.1103/PhysRevB.90.245127 PACS number(s): 71.10.Pm, 71.10.Fd

## I. INTRODUCTION

The spectral and dynamical properties of one-dimensional fermionic systems have attracted a significant amount of interest in recent years due to advances in both low-dimensional materials [1] and cold-atom systems [2]. The repulsive Hubbard model constitutes a key paradigm for studying strong correlation effects in these systems [3]. Its Hamiltonian is

$$H = -J\sum_{j,\sigma} c^\dagger_{j,\sigma}c_{j+1,\sigma} + c^\dagger_{j+1,\sigma}c_{j,\sigma} + U\sum_j n_{j,\uparrow}\,n_{j,\downarrow} - \mu\sum_j n_j, \tag{1}$$

where $n_{j,\sigma} = c^\dagger_{j,\sigma}c_{j,\sigma}$ and $n_j = n_{j,\uparrow} + n_{j,\downarrow}$. In one dimension, it is exactly solvable via the Bethe ansatz [3], with many results about the model available in the literature. However, the computation of dynamical correlation functions analytically and directly from the Bethe ansatz remains a difficult task. An example of particular interest is the single-particle spectral function:

$$A(\omega,k) = -\frac{1}{\pi}\,\mathrm{Im}\,G_{\mathrm{ret}}(\omega,k),$$
$$G_{\mathrm{ret}}(\omega,k) = -i\int_0^\infty dt\; e^{i\omega t}\sum_l e^{-ikla_0}\langle\psi_0|\{c_{j+l,\sigma}(t),\, c^\dagger_{j,\sigma}\}|\psi_0\rangle, \tag{2}$$

where $|\psi_0\rangle$ is the ground state. The spectral function is accessible through angle-resolved photoemission experiments. Such measurements on the quasi-1D organic conductor TTF-TCNQ have been interpreted in terms of $A(\omega,k)$ of the 1D Hubbard model [4,5].

One approach to calculating properties of the spectral function is via Luttinger liquid theory [6,7]. Certain low-energy aspects of the Hubbard model in zero magnetic field are described by the bosonized Hamiltonian $H = H_c + H_s$:

$$H = \sum_{\alpha=c,s}\frac{v_\alpha}{2\pi}\int dx\left[\frac{1}{K_\alpha}\left(\frac{\partial\Phi_\alpha}{\partial x}\right)^2 + K_\alpha\left(\frac{\partial\Theta_\alpha}{\partial x}\right)^2\right] + \ldots. \tag{3}$$

Here, the dots indicate the presence of *irrelevant* operators, which means that their respective coupling constants approach zero under the renormalization group flow. Neglecting the effects of the irrelevant operators in (3) makes it possible to calculate $A(\omega,k)$ at low energies [3,6–8]. The spectral function is found to exhibit singularities following the dispersions of the collective spin ("spinon") and charge ("holon") excitations. A problem with this Luttinger liquid approach to dynamical correlation functions is that the latter inherently involve a finite energy scale [e.g., the frequency $\omega$ in (2)], while the coupling constants of irrelevant perturbations (3) will, at best, be small but finite at the scale $\omega$.

In a number of works [9–25], it was demonstrated, for the case of spinless fermions, that taking the irrelevant operators perturbing the Luttinger liquid Hamiltonian into account generally leads to significant changes in the singularities characterizing the dominant features seen in response functions. Exact expressions for these singular features in response functions were obtained [9–17,20–22], using a mapping to a Luttinger liquid coupled to a mobile impurity [26]. Crucially, unlike in unperturbed Luttinger liquid theory, the exponents characterizing these singularities are generally *momentum dependent*. The generalization to spinful fermions, and the Hubbard model in particular, was considered in several recent works [27–31]. The case of the Mott-insulating phase beyond the field theory regime [32] was treated in Ref. [28], and a rather complete understanding of the dynamical structure factor was obtained.

For the metallic phase of the Hubbard model (less than one electron per site), a mobile impurity model was formulated to describe the singular features in the single-particle spectral function [29]. Combined with the Bethe ansatz solution, this allowed the calculation of exact expressions for the power-law singularities occurring at the "absolute threshold" [30]. These results were found to be in accord with previous analytic work based on completely different assumptions and methods [33]. On the other hand, a comparison of the analytic predictions [30] with available dynamical density matrix renormalization group (dDMRG) [34,35] results on the quarter-filled Hubbard model [5] was found to be rather unconvincing. A serious complication is that the dDMRG method used in Ref. [5] requires a finite imaginary part of the frequency, while the window in frequency space over which the calculated power law applies in general will be narrow. This makes extracting power-law singularities from dDMRG results in the momentum/frequency domain inherently difficult.

 

In this work, we employ a numerical approach to check the validity of the results for threshold singularities in response functions obtained by mobile impurity models. Using the time-evolving block decimation method (TEBD), formally equivalent to time-dependent density matrix renormalization group (tDMRG), cf. Refs. [36–38], we compute the retarded Green's function in the momentum/time domain for a variety of fillings and interaction strengths. As we will see, these results are well described by a fit to a power-law decay expression whose frequencies and exponents are fixed by combining Bethe ansatz results with an appropriate mobile impurity model.

The paper is organized as follows. In Sec. II, we present the single-particle spectrum through the spectral function $A(\omega,k)$ calculated using TEBD. In Sec. III, we identify its main features in terms of the exact excitation spectrum known from Bethe ansatz, and present results for edge exponents obtained from appropriate mobile impurity models. Implications of these findings for real-time dynamics are summarized in Sec. IV. Section V is devoted to a comparison of these results to the numerically calculated Green's function in the momentum/time domain. We summarize our results in Sec. VI.

## II. NUMERICAL STUDY OF THE SPECTRAL FUNCTION

We first use the DMRG algorithm to find the ground state $|\psi_0\rangle$ of the Hamiltonian (1) in an MPS representation. The TEBD algorithm is then used to obtain its dynamical properties (details of the numerical method used can be found in Refs. [34,36,39–41]). In particular, we calculate the retarded single-particle Green's function $G_{\rm ret}(\omega,k) = G^-(\omega,k) + G^+(\omega,k)$ from the Fourier transform for positive times of the dynamical two-point correlation functions

$$G^-(t,j) = -i\langle\psi_0|c_j^\dagger(t)c_{j_0}(0)|\psi_0\rangle, \quad (4)$$

$$G^+(t,j) = -i\langle\psi_0|c_j(t)c_{j_0}^\dagger(0)|\psi_0\rangle. \quad (5)$$

Each Green's function requires a separate simulation, performed by time-evolving an excited MPS, where an operator $c_{j_0}$ or $c_{j_0}^\dagger$ (the spin index is suppressed for clarity) has been applied at $t = 0$ to to the ground-state MPS, at the central site of a finite chain $j_0 = L/2$, see, e.g., Refs. [22,28,37]. We use open chains of length $L = 300$, and let the bond dimensions grow with time such that the truncation error is at most $10^{-5}$ per step. A fourth-order Suzuki-Trotter decomposition with time steps of $\sim$0.05 (in units of inverse hopping) is employed. The maximum time is chosen such that the wave-front of the "light-cone" of correlations does not reach the edges of the system, which introduces a cutoff at small frequencies. Before performing a Fourier transform of the data, the sampled time is extended using linear prediction [37], improving the energy resolution. In order to set the Fermi level at $\epsilon_F = 0$, the chemical potential $\mu$ in (1) is adjusted so that $E_0(N-1) = E_0(N)$, where $E_0(N)$ is the ground-state energy with $N$ electrons.

Throughout this paper we concentrate on the hole part of the Green's function (4), and consequently the presented spectral function only has support for negative frequencies $\omega < 0$. This spectral function is the quantity experimentally relevant to

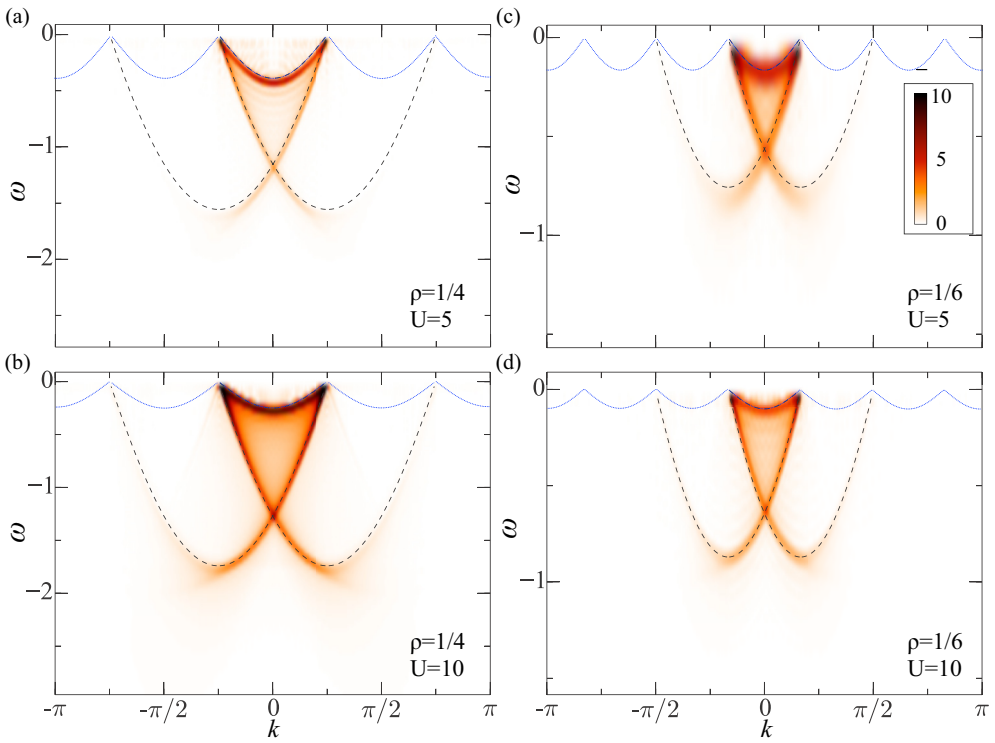


FIG. 1. (Color online) Spectral function $A(\omega,k)$ of the Hubbard model calculated with TEBD at filling $\rho = 1/4$ for (a) $U = 5$ and (b) $U = 10$ and at filling $\rho = 1/6$ for (a) $U = 5$ and (b) $U = 10$. The black dashed lines are the singularity thresholds obtained from the Bethe ansatz solution. In all cases, the spectral function is nonzero everywhere below the absolute threshold indicated by the thin blue lines, although the intensity is mostly very small.

photoemission spectra. The spectral function for filling factors $\rho = 1/4$ and $\rho = 1/6$ with interaction strengths $U = 5$ and 10 is shown in Fig. 1.

The main characteristics for $|k| < k_F$ can be clearly observed, as previously reported in, e.g., Ref. [5]. An injected fermion separates into (at least) one "spinon," a gapless spin-1/2 collective excitation with no charge, and one "(anti-)holon," a gapped, charged $\pm e$ collective excitation with no spin. The sharp line of the several $A(\omega,k)$ in Fig. 1 near $\omega = 0$ is the dispersion of the spinon excitation, while the lines below correspond to the holon excitations. Along these lines, $A(\omega,k)$ behaves as a power-law singularity. For a given total momentum, there exist holon-spinon states in a range of frequencies. These excitations are thoroughly described in the next section from the point of view of Bethe ansatz (dashed lines in Fig. 1). In the remainder of this paper, we will focus in analyzing the threshold singularities at the sharp edges for $|k| < k_F$. For $|k| > k_F$, there is a strong decay in the spectral weight and further features in the spectral function are difficult to observe for these parameters.

## III. EXCITATIONS IN THE HUBBARD MODEL AND DOMINANT FEATURES IN THE SPECTRAL FUNCTION

A detailed discussion of the excitation spectrum of the Hubbard model is given in Ref. [3] (see also Refs. [42]). The particular excitations relevant to the description of the single-particle Green's function have been constructed in detail in Ref. [30], and we now summarize the relevant results given there. We consider the case of zero magnetic field and $N$ electrons on an $L$-site periodic chain. The Fermi momentum is then

$$k_F = \frac{\pi N}{2L}. \tag{6}$$

The dominant features in the (hole) spectral function at momentum $|q| < k_F$ arise from the *holon-spinon* excitation carrying charge $+e$ and spin 1/2. Its energy and momentum are

$$\begin{aligned} E_{\rm hs}(k^h,\Lambda^h) &= -\varepsilon_c(k^h) - \varepsilon_s(\Lambda^h), \\ P_{\rm hs}(k^h,\Lambda^h) &= -p_c(k^h) - p_s(\Lambda^h) \pm 2k_F, \end{aligned} \tag{7}$$

where $|k^h| < Q$ and $-\infty < \Lambda^h < \infty$ parametrize the excitation. The functions $\varepsilon_{c,s}$ and $p_{c,s}$ are obtained from the solutions of coupled linear integral equations and are given in (19) and (28) of Ref. [30], respectively. The origin of the $\pm 2k_F$ contribution is discussed in Chapter 7.7.1. of Ref. [3]. Because of parity invariance the Green's function is symmetric in momentum and we therefore restrict ourselves to the momentum range

$$0 \leqslant P_{\rm hs} \leqslant k_F. \tag{8}$$

### A. Absolute threshold: spinon edge

The absolute threshold for $0 < P_{\rm hs} < k_F$ was analyzed in detail in Ref. [30]. It is obtained by choosing the plus sign in (7), fixing $k_h = Q$, and then varying $\Lambda^h$ in the range

$$-\infty < \Lambda^h \leqslant 0. \tag{9}$$

At energies just above this threshold, the spectral function exhibits a power-law singularity [29,30] (as a function of frequency for fixed momentum)

$$A(\omega, P_{\rm hs}(Q,\Lambda^h)) \propto (\omega - E_{\rm hs}(Q,\Lambda^h))^{-\mu^s_{0,-}}, \tag{10}$$

where the exponent $\mu^s_{0,-}$ is given in (129) of Ref. [30].

### B. Holon edge

The other dominant features in the spectral function arise in the vicinity of the holon edge, obtained by choosing the minus sign in (7), setting $\Lambda^h = -\infty$ and varying $k^h$ in the range

$$-Q \leqslant k^h < 0. \tag{11}$$

The range of the corresponding momentum is $-k_F \leqslant P_{\rm hs} < k_F$. We note that by virtue of parity invariance this particular branch is sufficient for describing both high-energy features in the spectral function $A(\omega,0 < q < k_F)$. We now assume that, as a consequence of the integrability of the Hubbard model, a threshold singularity occurs just above the holon edge (as a function of frequency for fixed momentum)

$$A(\omega, P_{\rm hs}(k^h, -\infty)) \propto (\omega - E_{\rm hs}(k^h, -\infty))^{-\mu^c_{0,-}}. \tag{12}$$

The assumption that in integrable models threshold singularities occur even at thresholds of excitations that sit on top of continua, into which they are kinematically allowed to decay, appears reasonable; for massive integrable quantum field theories, this has been seen to be the case [43]. In nonintegrable models one does not expect singular behavior [29].

The exponent $\mu^c_{0,-}$ can then be calculated in the framework of a mobile impurity model using input from the Bethe ansatz solution. Some details of this calculation are given in Appendix. The result for the threshold exponent is

$$\mu^c_{0,-} = \frac{1}{2} - K_c\left(\frac{1}{2} - 2D_c^{\rm imp}\right)^2 - \frac{\left(N_c^{\rm imp}\right)^2}{4K_c}, \tag{13}$$

where $K_c$ is the Luttinger liquid parameter (cf. (119) and (103) of Ref. [30]),

$$\begin{aligned} N_c^{\rm imp} &= \int_{-Q}^{Q} {\rm d}k\ \rho_{c,1}(k), \\ 2D_c^{\rm imp} &= \Phi(k^h) + \int_{Q}^{\pi} {\rm d}k\ [\rho_{c,1}(-k) - \rho_{c,1}(k)] \\ &\quad - \int_{-Q}^{Q} {\rm d}k\ \rho_{c,1}(k)\ \Phi(k), \\ \Phi(k) &= \frac{i}{\pi} \ln\left[\frac{\Gamma\left(\frac{1}{2} + i\frac{\sin k}{4u}\right)\Gamma\left(1 - i\frac{\sin k}{4u}\right)}{\Gamma\left(\frac{1}{2} - i\frac{\sin k}{4u}\right)\Gamma\left(1 + i\frac{\sin k}{4u}\right)}\right], \end{aligned} \tag{14}$$

and the function $\rho_{c,1}$ is the solution of the integral equation

$$\begin{aligned} \rho_{c,1}(k) &= -\cos k\ R(\sin k - \sin k^h) \\ &\quad + \cos k \int_{-Q}^{Q} {\rm d}k' R(\sin k - \sin k')\rho_{c,1}(k'). \end{aligned} \tag{15}$$

Here, $u = U/4$ and

$$R(x) = \int_{-\infty}^{\infty} \frac{d\omega}{2\pi} \frac{e^{i\omega x}}{1 + \exp(2u|\omega|)}. \tag{16}$$

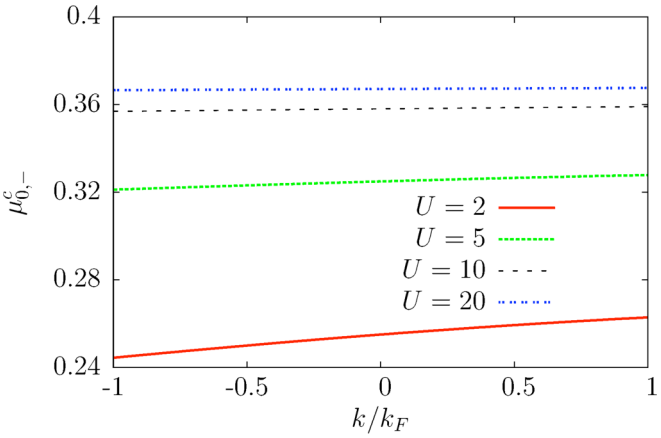


FIG. 2. (Color online) Exponent $\mu^c_{0,-}$ for $\rho = 1/4$ as a function of momentum as derived from the mobile impurity model approach for various fillings and values of $U$.

In Figs. 2 and 3, we plot the value of the exponent $\mu^c_{0,-}$ as a function of momentum for several values of interaction strength $U$ and band fillings $1/4$ and $1/6$, respectively. We note that our results are again in accord with those of Ref. [33].

## IV. MOBILE IMPURITY MODEL AND REAL-TIME DYNAMICS

We have seen above that for a given momentum $0 < |k| < k_F$ the single-particle spectral function exhibits threshold singularities at frequencies

$$\begin{aligned} \omega_1 &= E_{\rm hs}(Q,\Lambda^h), \quad P_{\rm hs}(Q,\Lambda^h) = k, \\ \omega_2 &= E_{\rm hs}(k^h,-\infty), \quad P_{\rm hs}(k^h,-\infty) = k, \\ \omega_3 &= E_{\rm hs}(k^h,-\infty), \quad P_{\rm hs}(k^h,-\infty) = -k. \end{aligned} \tag{17}$$

Assuming that the singular features in the spectral function give the dominant behavior of the retarded Green's function at late times, we conclude that the latter should be

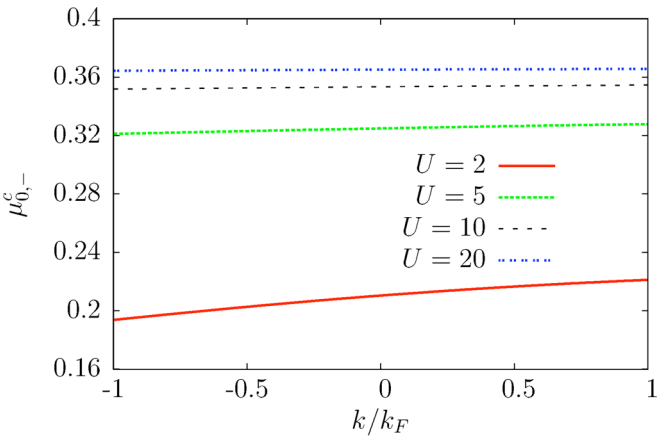


FIG. 3. (Color online) Exponent $\mu^c_{0,-}$ for $\rho = 1/6$ as a function of momentum as derived from the mobile impurity model approach for various fillings and values of $U$.

TABLE I. Values for the parameters of the power-law decay function (18), calculated from the Bethe ansatz and mobility impurity model.

| $\rho$ | $U$ | $k$ | $-\omega_1$ | $-\omega_2$ | $-\omega_3$ | $\mu^c_{0,-}$ | $\mu^s_{0,-}$ |
|---|---|---|---|---|---|---|---|
| 1/4 | 5 | 0 | 0.387 | 1.15 | 1.15 | 0.373 | 0.855 |
| 1/4 | 5 | $\pi/8$ | 0.277 | 0.661 | 1.46 | 0.392 | 0.782 |
| 1/4 | 10 | 0 | 0.245 | 0.245 | 1.27 | 0.378 | 0.732 |
| 1/4 | 10 | $\pi/8$ | 0.178 | 0.713 | 1.62 | 0.388 | 0.660 |
| 1/6 | 5 | 0 | 0.165 | 0.564 | 0.564 | 0.325 | 0.851 |
| 1/6 | 5 | $\pi/8$ | 0.0631 | 0.173 | 0.745 | 0.237 | 0.632 |
| 1/6 | 10 | 0 | 0.101 | 0.644 | 0.644 | 0.353 | 0.710 |
| 1/6 | 10 | $\pi/8$ | 0.0384 | 0.195 | 0.856 | 0.354 | 0.545 |

(approximately) of the form

$$G(t,k) \sim \sum_\alpha A_\alpha e^{i\omega_\alpha t + \phi_\alpha} t^{-\gamma_\alpha}, \tag{18}$$

where the threshold exponents $\gamma_\alpha$ are related $\gamma_\alpha = \mu^{c/s}_{0,-} + 1$ to the exponents calculated with the mobile impurity method. All parameters are a function of momentum $k$. Here, $A_\alpha$ are complex amplitudes and $\phi_\alpha$ are real phases. It is currently not known how to determine them *a priori*, see however

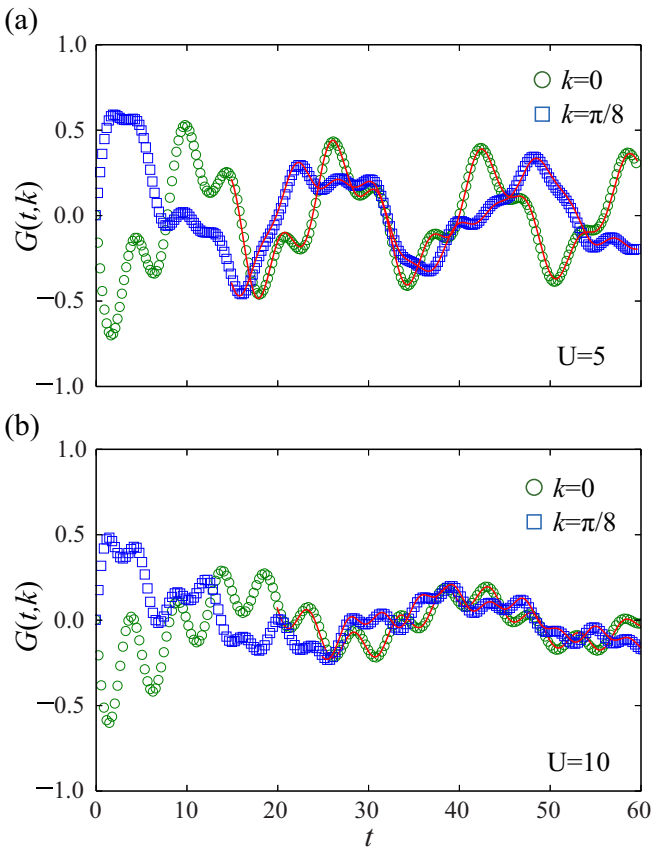


FIG. 4. (Color online) Time decay of the imaginary part of the Green's function $G(t,k)$ for filling $\rho = 1/4$. Symbols are numerical TEBD data and red lines are fits to the power-law decay of the form of (18).

Ref. [44]. Table I gives explicit values for the frequencies $\omega_\alpha$ and exponents $\mu_\alpha$, to be compared with TEBD results.

## V. COMPARISON WITH NUMERICAL RESULTS

The formula (18) for $G(t,k)$ has too many free parameters to reliably fit the numerical data from TEBD simulations, obtained through a Fourier transform of the (hole) Green's function (4). Therefore we fix the threshold frequencies $\omega_\alpha$ and the exponents $\gamma_\alpha$ to the values calculated with the mobile impurity approach, leaving the momentum-dependent amplitudes and phases as the only free parameters. We fit the imaginary part of $G(t,k)$ to the ansatz but the procedure holds equally well with the real part. The data used for the fitting procedure are not extended in time with linear prediction. The time evolution of the Green's function is illustrated for $\rho = 1/4$ in Fig. 4 for $U = 5$ and 10, both at $k = 0$ and $\pi/8$. The initial time of the fit is adjusted in each case in order to avoid nonuniversal behavior at short times. For later times, the decay of $G(t,k)$ is very well reproduced by the fitting ansatz (18). The good quality of the fits to the numerical data is the main result of our paper, which validates the mobile impurity approach. As the momenta approaches $k_F$, the quality of the fit worsens slightly. One can understand this, since the frequency at which the first singularity develops approaches $\omega \to 0$, which is more difficult to capture with a TEBD approach, inherently limited to a given finite time.

TABLE II. Fiting parameters of the power-law decay function (18) to the time decay of the Green's function calculated numerically with TEBD.

| $\rho$ | $U$ | $k$ | $A_1$ | $A_2$ | $A_3$ | $\phi_1$ | $\phi_2$ | $\phi_3$ |
|---|---|---|---|---|---|---|---|---|
| 1/4 | 5 | 0 | 0.54 | 0.50 | 0.57 | 4.16 | 4.13 | 4.6 |
| 1/4 | 5 | $\pi/8$ | 0.57 | 0.71 | 0.34 | 1.03 | 5.1 | 3.74 |
| 1/4 | 10 | 0 | 0.39 | 0.94 | 1.02 | 3.83 | 0.25 | 3.62 |
| 1/4 | 10 | $\pi/8$ | 0.45 | 0.54 | 0.36 | 0.85 | 2.01 | 1.09 |
| 1/6 | 5 | 0 | 0.68 | 4.48 | 1.83 | 6.02 | 3.64 | 4.25 |
| 1/6 | 5 | $\pi/8$ | 0.76 | 2.00 | 0.47 | 1.42 | 2.41 | 6.06 |
| 1/6 | 10 | 0 | 0.46 | 2.38 | 3.29 | 4.62 | 3.14 | 0.38 |
| 1/6 | 10 | $\pi/8$ | 1.55 | 0.64 | 0.31 | 1.66 | 2.69 | 1.34 |

The same behavior is essentially observed for $\rho = 1/6$ in Fig. 5. The relaxation to a universal behavior is slower for $\rho = 1/6$, which agrees with the poorer resolution in frequency space observed in Fig. 1. Table II gives explicit values for the obtained fitting paramaters $A_\alpha$ and $\phi_\alpha$ for the range of parameters studied here.

As the fitting approach nicely reproduces the long-time behavior, we can use it instead of linear prediction to extend the raw TEBD data to longer times. In the combined TEBD+BA

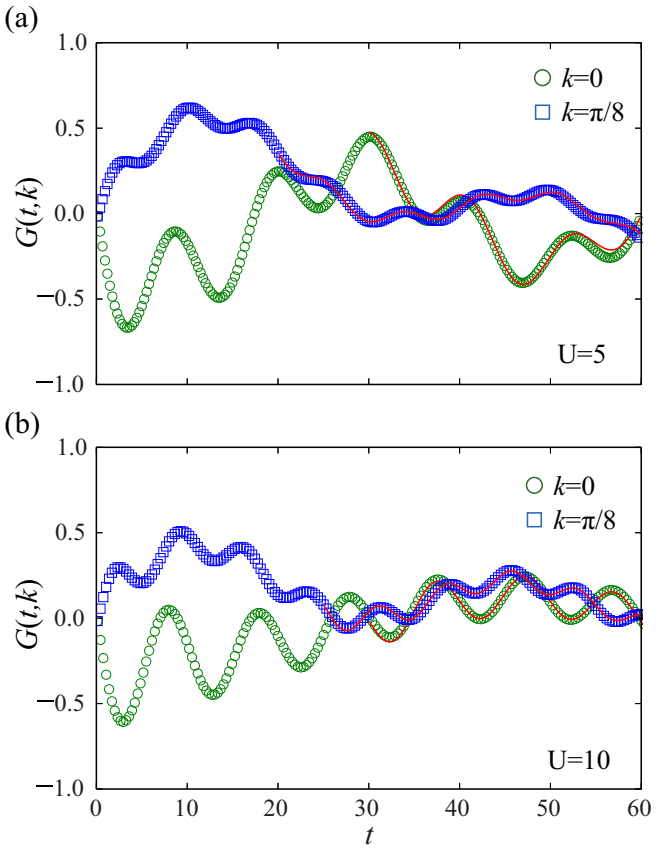


FIG. 5. (Color online) Time decay of the imaginary part of the Green's function $G(t,k)$ for filling $\rho = 1/6$. Symbols are numerical TEBD data and red lines are fits to the power-law decay of the form of (18).

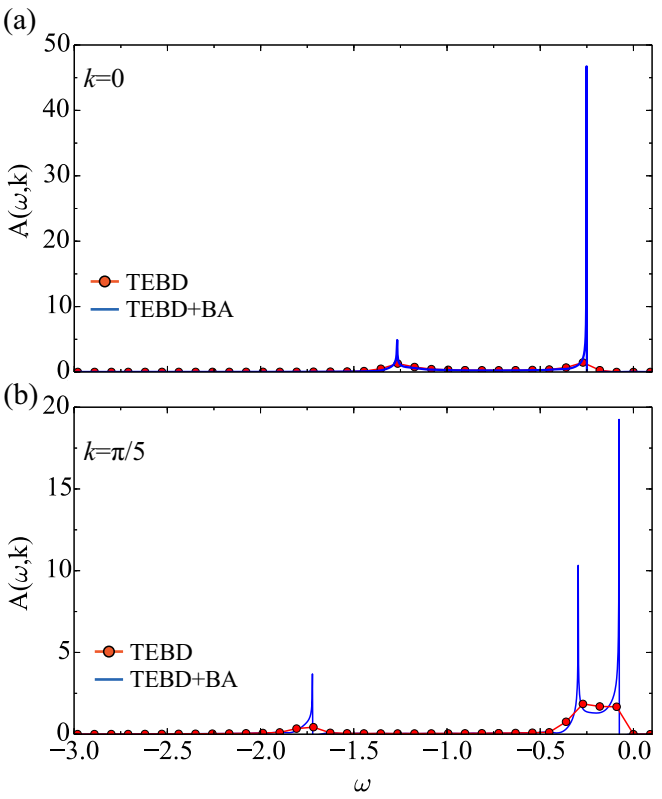


FIG. 6. (Color online) Comparison between the spectral function $A(\omega,k)$ at fixed momentum $k$ calculated with raw TEBD data (red) and TEBD extended in time with ansatz (18) with BA and mobile impurity model parameters (blue). Results for quarter filling and $U = 10$.

approach, we extrapolate the real-time data by orders of magnitude using the ansatz (18) with parameters taken from the analytical approach and the fitting procedure outlined above. Such a combined method dramatically increases the frequency resolution of the resulting spectral function with clearly defined singularity peaks, as show in Fig. 6, for the case of $\rho = 1/4$ and $U = 10$. The spectral functions from both approaches have been normalized to obey the momentum-distribution function sum rule $\int_{-\infty}^{0} A(\omega,k) = n(k)$.

## VI. CONCLUSIONS

In this work, we have studied the single particle Green's function $G(t,k)$ of the one-dimensional repulsive Hubbard model in the metallic regime. Using matrix product state techniques, we computed $G(t,k)$ for a variety of band fillings and interaction strengths for large systems ($L = 300$) and times $0 < t \lesssim 60$ (in units of inverse hopping). We then employed mobile impurity models in tandem with the Bethe ansatz solution to obtain an expression for the late time asymptotic behavior of the Green's function. Using the unknown coefficients in the resulting expression as fit parameters, we obtained an excellent agreement with the numerical results at late times. This strongly suggests that the mobile impurity results are not only correct, but are of practical value. Moreover, it removes concerns based on the poor agreement between threshold singularity exponents (in the frequency domain) obtained by mobile impurity models [30] and earlier dynamical DMRG computations [5]. Finally, we have shown that, combining the numerical results at short and intermediate times with the asymptotic form dictated by the mobile impurity model, it is possible to obtain results for the single particle spectral function with unprecedented frequency resolution. We expect this observation to be of practical use also in further cases.

## ACKNOWLEDGMENTS

This work was supported in part by the EPSRC under grants EP/I032487/1 (FHLE and TV) and EP/J014885/1 (FHLE and TV), and by the DFG under the Grant SCHN 1169/2-1 (IS).

## APPENDIX: CALCULATION OF THE HOLON EDGE EXPONENT

In this Appendix, we summarize the technical details underlying our calculation of edge exponents in the framework of mobile impurity models. In order to simplify the notation, we introduce the convolution $*$:

$$\begin{aligned} K * f|_k &= \int_{-Q}^{Q} dq\ K(k,q)\ f(q), \\ K(k,q) &= \cos(k)\ R[\sin(k) - \sin(q)], \end{aligned} \tag{A1}$$

where the function $R(x)$ is given in (16). The action of the transposed integral operator $K^T$ is defined by replacing $K(k,q)$ by $K(q,k)$ on the right-hand side of (A1).

### 1. Finite-size energy levels

A key input in determining edge exponents is the finite-size excitation spectrum in presence of a high-energy holon. The latter can be obtained in a complete analogy to the calculation of the excitation spectrum in the vicinity of the spinon edge in Ref. [30]. The result of this calculation is

$$\begin{aligned} &E(\Delta N_c, \Delta N_s, D_c, D_s) \\ &\quad = L e_{\mathrm{GS}} - \varepsilon_c(k^h) - \frac{\pi}{6L}(v_s + v_c) - \frac{1}{L}\varepsilon_c'(k^h)\delta k^h \\ &\qquad + \frac{2\pi v_c}{L}\left[\frac{\left(\Delta N_c - N_c^{\mathrm{imp}}\right)^2}{4\xi^2}\right. \\ &\qquad \left. + \xi^2\left(D_c - D_c^{\mathrm{imp}} + \frac{D_s}{2} - \frac{D_s^{\mathrm{imp}}}{2}\right)^2\right] \\ &\qquad + \frac{2\pi v_s}{L}\left[\frac{1}{2}\left(\Delta N_s - \frac{\Delta N_c}{2} - N_s^{\mathrm{imp}} + \frac{N_c^{\mathrm{imp}}}{2}\right)^2\right. \\ &\qquad \left. + \frac{\left(D_s - D_s^{\mathrm{imp}}\right)^2}{2}\right]. \end{aligned} \tag{A2}$$

The various quantities entering (A2) are as follows. (1) The dressed energy for holons $\varepsilon_c(k)$ is a solution to the integral equation

$$\varepsilon_c(k) = -2\cos(k) - \mu - 2u + K^T * \varepsilon_c|_k. \tag{A3}$$

The integration boundary $Q$ is fixed by the requirement $\varepsilon_c(\pm Q) = 0$.

(2) $\varepsilon_c'(k)$ is the derivative of $\varepsilon_c(k)$ with respect to $k$.

(3) $e_{\mathrm{GS}}$ is the ground-state energy per site:

$$e_{\mathrm{GS}} = \int_{-Q}^{Q} \frac{dk}{2\pi}\ \varepsilon_c(k) + u. \tag{A4}$$

(4) The spin and charge velocities $v_{s,c}$ are obtained as

$$\begin{aligned} v_s &= \frac{\varepsilon_s'(\infty)}{2\pi\rho_s(\infty)}, \quad v_c = \frac{\varepsilon_c'(Q)}{2\pi\rho_c(Q)}, \\ \varepsilon_s(\Lambda) &= \int_{-Q}^{Q} dk\,\cos(k)\ s(\Lambda - \sin(k))\ \varepsilon_c(k), \\ \rho_c(k) &= \frac{1}{2\pi} + K * \rho_c\Big|_k, \\ \rho_s(\Lambda) &= \int_{-Q}^{Q} dk\ s(\Lambda - \sin(k))\ \rho_c(k), \end{aligned} \tag{A5}$$

where $s(x) = [4u\cosh(\frac{\pi x}{2u})]^{-1}$.

(5) The dressed charge $\xi = \xi(Q)$ is obtained from the solution of the integral equation

$$\xi(k) = 1 + K^T * \xi\Big|_k. \tag{A6}$$

(6) $\Delta N_{c,s}$ and $D_{c,s}$ are quantum numbers describing the excitation under consideration. If we only have a high-energy holon with rapidity $k^h$ and a low-energy spinon sitting at its

Fermi point $\Lambda^h = -\infty$, then

$$\Delta N_c = 0\ ,\ \Delta N_s = -1\ ,\ D_s = -D_c = \tfrac{1}{2}. \tag{A7}$$

The identification (A7) follows from the definition of $\Delta N_{c,s}$ and $D_{c,s}$ in terms of the (half-odd) integers characterizing a given solution of the Bethe ansatz equation, cf Ref. [30].

(7) The quantities $N_{c,s}^{\rm imp}$ and $D_{c,s}^{\rm imp}$ are given by

$$\begin{aligned} N_c^{\rm imp} &= \int_{-Q}^{Q} {\rm d}k\ \rho_{c,1}(k), \\ N_s^{\rm imp} &= \int_{-\infty}^{\infty} {\rm d}\Lambda\ \rho_{s,1}(\Lambda) = \frac{1}{2}\big(N_c^{\rm imp} - 1\big), \\ 2D_c^{\rm imp} &= \int_{Q}^{\pi} {\rm d}k\ [\rho_{c,1}(-k) - \rho_{c,1}(k)] \\ &\quad + \frac{i}{\pi} \ln\left[\frac{\Gamma\big(\frac{1}{2} + i\frac{\sin k^h}{4u}\big)\Gamma\big(1 - i\frac{\sin k^h}{4u}\big)}{\Gamma\big(\frac{1}{2} - i\frac{\sin k^h}{4u}\big)\Gamma\big(1 + i\frac{\sin k^h}{4u}\big)}\right] \\ &\quad - \frac{i}{\pi}\int_{-Q}^{Q} {\rm d}k\ \rho_{c,1}(k) \\ &\quad \times \ln\left[\frac{\Gamma\big(\frac{1}{2} + i\frac{\sin k}{4u}\big)\Gamma\big(1 - i\frac{\sin k}{4u}\big)}{\Gamma\big(\frac{1}{2} - i\frac{\sin k}{4u}\big)\Gamma\big(1 + i\frac{\sin k}{4u}\big)}\right], \\ D_s^{\rm imp} &= 0. \end{aligned} \tag{A8, A9}$$

(8) The "order 1" part $k^h$ of the holon rapidity is determined by the requirement

$$\begin{aligned} z_c(k^h) &= k^h + \int_{-\infty}^{\infty} {\rm d}\Lambda\ \rho_s(\Lambda)\,\theta\left(\frac{\sin k^h - \Lambda}{u}\right) \\ &= \frac{2\pi I^h}{L}, \end{aligned} \tag{A10}$$

where $I^h$ is a (half-odd) integer number characterizing the momentum of the holon.

(9) The parameter $\delta k^h$ describes the "order $1/L$" part of holon rapidity in the finite volume, and for zero magnetic field is given by

$$\begin{aligned} \rho_{c,0}(k^h)\delta k^h &= -\int_{-\infty}^{\infty} \frac{{\rm d}\Lambda}{2\pi}\ \rho_{s,1}(\Lambda)\,\theta\left(\frac{\sin k^h - \Lambda}{u}\right) \\ &\quad - \int_{-\infty}^{\infty} \frac{{\rm d}\Lambda}{2\pi} \sum_{\sigma=\pm} r_{sc}^{(\sigma)}(\Lambda)\,\theta\left(\frac{\sin k^h - \Lambda}{u}\right) \\ &\quad \times (Q_\sigma - \sigma Q) + \frac{1}{2\sqrt{2}}, \end{aligned} \tag{A11}$$

where the quantities $r_{\alpha c}^{(\sigma)}(z)$ satisfy

$$\begin{aligned} r_{cc}^{(\sigma)}(k) &= K * r_{cc}^{(\sigma)}\Big|_k + \sigma K(k, \sigma Q), \\ r_{sc}^{(\sigma)}(\Lambda) &= \int_{-Q}^{Q} {\rm d}k\, s(\Lambda - \sin k)\, r_{cc}^{(\sigma)}(k) \\ &\quad + \sigma s(\Lambda - \sigma \sin Q). \end{aligned} \tag{A12}$$

### 2. Impurity model and field theory

The appropriate mobile impurity model for describing the holon edge is [29] $H_c + H_s + H_{\rm int} + H_d$, where

$$H_\alpha = \frac{v_\alpha}{2\pi}\int dx \left[\frac{1}{K_\alpha}\left(\frac{\partial \Phi_\alpha}{\partial x}\right)^2 + K_\alpha\left(\frac{\partial \Theta_\alpha}{\partial x}\right)^2\right], \tag{A13}$$

$$\begin{aligned} H_{\rm int} &= \int dx\ \left[\frac{V_R - V_L}{2\pi}\partial_x \Theta_c - \frac{V_R + V_L}{2\pi}\partial_x \Phi_c\right] dd^\dagger, \\ H_d &= \int dx\ d^\dagger(x)[\varepsilon_c(P) - iu\partial_x]d(x). \end{aligned} \tag{A14}$$

Here, the Bose fields $\Phi_\alpha$ and the dual fields $\Theta_\alpha$ fulfill the commutation relations $[\Phi_\alpha(x), \frac{\partial\Theta_\beta(y)}{\partial y}] = i\pi\delta_{\alpha\beta}\delta(x-y)$, $d(x)$ and $d^\dagger(x)$ are annihilation and creation operators of the mobile impurity, which carries momentum $P$ and travels at velocity $u$. The parameters $V_{R,L}$ characterize the interaction of the impurity with the low-energy charge degrees of freedom. The parameters of $H_{c,s}$ and $H_d$ in (A14) are readily identified with quantities obtained from the Bethe ansatz. The spin and charge velocities $v_{s,c}$ are given by (A5) and the Luttinger parameters are

$$K_s = 1, \quad K_c = \frac{\xi^2}{2}, \tag{A15}$$

where $\xi$ is given by (A6). The velocity of the impurity is expressed in terms of the solutions to the integral equations (A3) and (A5) as

$$u = \frac{\varepsilon_c'(k^h)}{2\pi\rho_c(k^h)}. \tag{A16}$$

The position $k^h$ of the hole is fixed by the requirement

$$P_{hs}(k^h) = P. \tag{A17}$$

The parameters $V_{R,L}$ entering the expression for $H_{\rm int}$ are determined as follows. Following Ref. [29], we remove the interaction term $H_{\rm int}$ through the unitary transformation $U^\dagger H U$

$$\begin{aligned} U^\dagger = \exp\Bigg\{-i\int dx\Bigg[&\sqrt{K_c}\frac{\Delta\delta_{+,c} - \Delta\delta_{-,c}}{2\pi}\Theta_c(x) \\ &- \frac{\Delta\delta_{+,c} + \Delta\delta_{-,c}}{2\pi\sqrt{K_c}}\Phi_c(x)\Bigg] d(x)d^\dagger(x)\Bigg\}, \end{aligned} \tag{A18}$$

where

$$(V_L \mp V_R)K_c^{\mp\frac{1}{2}} = (v_c + u)\Delta\delta_{-,c} \pm (v_c - u)\Delta\delta_{+,c}. \tag{A19}$$

In the resulting Hamiltonian, the impurity no longer interacts explicitly with the charge part of Luttinger liquid, which in the transformed basis takes the form

$$U^\dagger H_c U = \frac{v_c}{2\pi}\int dx \left[\frac{1}{K_c}\left(\frac{\partial \widehat{\Phi}_c}{\partial x}\right)^2 + K_c\left(\frac{\partial \widehat{\Theta}_c}{\partial x}\right)^2\right]. \tag{A20}$$

The main effect of the unitary transformation is to change the boundary conditions of the charge boson. In particular, one

has

$$\partial_x \widehat{\Phi}_c = U^\dagger \partial_x \Phi_c U = \partial_x \Phi_c + \frac{\sqrt{K_c}}{2}(\Delta\delta_{+,c} - \Delta\delta_{-,c})dd^\dagger,$$
$$\partial_x \widehat{\Theta}_c = U^\dagger \partial_x \Theta_c U = \partial_x \Theta_c - \frac{1}{2\sqrt{K_c}}(\Delta\delta_{+,c} + \Delta\delta_{-,c})dd^\dagger. \tag{A21}$$

Equations (A21) imply that the finite-size spectrum of (A20) in presence of a high-energy holon impurity can be cast in the form

$$\Delta E = \frac{2\pi v_c}{L}\left[\frac{\left(m_c + \bar{m}_c + \sqrt{2K_c}\frac{\Delta\delta_{c,+}-\Delta\delta_{c,-}}{2\pi}\right)^2}{8K_c} + \frac{K_c}{8}\left(m_c - \bar{m}_c - \sqrt{\frac{2}{K_c}}\frac{\Delta\delta_{c,+}+\Delta\delta_{c,-}}{2\pi}\right)^2 + \sum_{n>0} n(M^+_{n,c} + M^-_{n,c})\right] + \frac{2\pi v_s}{L}\left[\left(\frac{m_s}{2}\right)^2 + \left(\frac{\bar{m}_s}{2}\right)^2 + \sum_{n>0} n(M^+_{n,s} + M^-_{n,s})\right], \tag{A22}$$

see, e.g., Ref. [45], where

$$m_\alpha + \bar{m}_\alpha = -\frac{\sqrt{2}}{\pi}\int dx\ \langle \partial_x \Phi_\alpha \rangle,$$
$$m_\alpha - \bar{m}_\alpha = \frac{\sqrt{2}}{\pi}\int dx\ \langle \partial_x \Theta_\alpha \rangle, \quad \alpha = c,s. \tag{A23}$$

For the holon edge threshold, we have

$$m_c = \bar{m}_c = 0, \quad m_s = -1, \quad \bar{m}_s = 0. \tag{A24}$$

Comparing the resulting energies to the Bethe Ansatz form (A2), we conclude that

$$N_c^{\rm imp} = -\sqrt{2K_c}\frac{\Delta\delta_{c,+} - \Delta\delta_{c,-}}{2\pi},$$
$$2D_c^{\rm imp} = -\frac{1}{2} + \frac{1}{\sqrt{2K_c}}\frac{\Delta\delta_{c,+} + \Delta\delta_{c,-}}{2\pi}. \tag{A25}$$

### 3. Holon edge exponent

Given the phase shifts $\Delta\delta_{c,\pm}$ the holon edge exponent can be obtained following Ref. [29]. The result is

$$\mu^c_{0,-} = \frac{1}{2} - K_c\left(\frac{1}{2} - 2D_c^{\rm imp}\right)^2 - \frac{\left(N_c^{\rm imp}\right)^2}{4K_c}. \tag{A26}$$

It is useful to consider particular limiting cases.

(1) Infinite interaction limit $u \to \infty$

$$\lim_{u\to\infty} \mu^c_{0,-} = \frac{1}{2} - \frac{K_c}{4} = \frac{3}{8}. \tag{A27}$$

As expected, this agrees with Ref. [29].

(2) $k \to k_F$ limit: here the result is

$$\lim_{k\to k_F} \mu^c_{0,-} = \frac{1}{2} - K_c\left(\frac{1}{2} - \frac{1}{\sqrt{2K_c}}\right)^2 - \frac{\left(1-\sqrt{2K_c}\right)^2}{4K_c}. \tag{A28}$$

This again agrees with Ref. [29] and is *different* from the Luttinger liquid result

$$\mu^c_{-} = \frac{1}{2} - \frac{1}{8}\left(K_c + \frac{1}{K_c} - 2\right). \tag{A29}$$


[1] *Strong Interactions in Low Dimensions*, edited by D. Baeriswyl and L. Degiorgi (Kluwer, Dordrecht, 2004).
[2] I. Bloch, J. Dalibard, and S. Nascimbène, Nat. Phys. **8**, 267 (2012).
[3] F. H. L. Essler, H. Frahm, F. Göhmann, A. Klümper, and V. E. Korepin, *The One-Dimensional Hubbard Model* (Cambridge University Press, Cambridge, 2005).
[4] R. Claessen, M. Sing, U. Schwingenschlögl, P. Blaha, M. Dressel, and C. S. Jacobsen, Phys. Rev. Lett. **88**, 096402 (2002).
[5] H. Benthien, F. Gebhard, and E. Jeckelmann, Phys. Rev. Lett. **92**, 256401 (2004).
[6] A. O. Gogolin, A. A. Nersesyan, and A. M. Tsvelik, *Bosonization in Strongly Correlated Systems* (Cambridge University Press, 1999).
[7] T. Giamarchi, *Quantum Physics in One Dimension* (Oxford University Press, New York, 2004).
[8] V. Meden and K. Schönhammer, Phys. Rev. B **46**, 15753 (1992); J. Voit, *ibid.* **47**, 6740 (1993).
[9] M. Pustilnik, M. Khodas, A. Kamenev, and L. I. Glazman, Phys. Rev. Lett. **96**, 196405 (2006).
[10] A. V. Rozhkov, Phys. Rev. B **74**, 245123 (2006).
[11] R. G. Pereira, J. Sirker, J.-S. Caux, R. Hagemans, J. M. Maillet, S. R. White, and I. Affleck, Phys. Rev. Lett. **96**, 257202 (2006).
[12] E. Bettelheim, A. G. Abanov, and P. Wiegmann, Phys. Rev. Lett. **97**, 246401 (2006).
[13] M. Khodas, M. Pustilnik, A. Kamenev, and L. I. Glazman, Phys. Rev. Lett. **99**, 110405 (2007).
[14] M. Khodas, M. Pustilnik, A. Kamenev, and L. I. Glazman, Phys. Rev. B **76**, 155402 (2007).
[15] R. G. Pereira, S. R. White, and I. Affleck, Phys. Rev. Lett. **100**, 027206 (2008).
[16] A. Imambekov and L. I. Glazman, Phys. Rev. Lett. **100**, 206805 (2008).
[17] V. V. Cheianov and M. Pustilnik, Phys. Rev. Lett. **100**, 126403 (2008).
[18] E. Bettelheim, A. G. Abanov, and P. Wiegmann, J. Phys. A **41**, 392003 (2008).
[19] A. G. Abanov, E. Bettelheim, and P. Wiegmann, J. Phys. A **42**, 135201 (2009).
[20] A. Imambekov and L. I. Glazman, Phys. Rev. Lett. **102**, 126405 (2009).
[21] A. Imambekov and L. I. Glazman, Science **323**, 228 (2009).

[22] R. G. Pereira, S. R. White, and I. Affleck, Phys. Rev. B **79**, 165113 (2009).
[23] R. G. Pereira, Int. J. Mod. Phys. B **26**, 1244008 (2012).
[24] A. V. Rozhkov, Phys. Rev. Lett. **112**, 106403 (2014).
[25] T. Price and A. Lamacraft, arXiv:1405.7372.
[26] L. Balents, Phys. Rev. B **61**, 4429 (2000).
[27] E. Sela and R. G. Pereira, Phys. Rev. B **84**, 014407 (2011).
[28] R. G. Pereira, K. Penc, S. R. White, P. D. Sacramento, and J. M. P. Carmelo, Phys. Rev. B **85**, 165132 (2012).
[29] T. L. Schmidt, A. Imambekov, and L. I. Glazman, Phys. Rev. Lett. **104**, 116403 (2010); Phys. Rev. B **82**, 245104 (2010); A. Imambekov, T. L. Schmidt, and L. I. Glazman, Rev. Mod. Phys **84**, 1253 (2012).
[30] F. H. L. Essler, Phys. Rev. B **81**, 205120 (2010).
[31] O. Tsyplyatyev and A. J. Schofield, Phys. Rev. B **90**, 014309 (2014).
[32] P. B. Wiegmann, Sov. Sci. Rev. Ser. A **2**, 41 (1980); J. Voit, Eur. Phys. J. B **5**, 505 (1998); E. Jeckelmann, F. Gebhard, and F. H. L. Essler, Phys. Rev. Lett. **85**, 3910 (2000); F. H. L. Essler and A. M. Tsvelik, Phys. Rev. B **65**, 115117 (2002); D. Controzzi and F. H. L. Essler, *ibid.* **66**, 165112 (2002); B. Doyon and S. Lukyanov, Nucl. Phys. B **644**, 451 (2002).
[33] J. M. P. Carmelo, K. Penc, L. M. Martelo, P. D. Sacramento, J. M. B. Lopes Dos Santos, R. Claessen, M. Sing, and U. Schwingenschlögl, Europhys. Lett. **67**, 233 (2004); J. M. P. Carmelo, K. Penc, and D. Bozi, Nucl. Phys. B **725**, 421 (2005); J. M. P. Carmelo, K. Penc, P. D. Sacramento, M. Sing, and R. Claessen, J. Phys.: Cond. Matter **18**, 5191 (2006); J. M. P. Carmelo, K. Penc, and D. Bozi, Nucl. Phys. B **737**, 351 (2006); J. M. P. Carmelo, D. Bozi, and K. Penc, J. Phys. Cond. Mat. **20**, 415103 (2008).
[34] S. R. White, Phys. Rev. Lett. **69**, 2863 (1992).
[35] E. Jeckelmann, Phys. Rev. B **66**, 045114 (2002).
[36] G. Vidal, Phys. Rev. Lett. **93**, 040502 (2004)
[37] S. R. White and I. Affleck, Phys. Rev. B **77**, 134437 (2008).
[38] Ulrich Schollwöck, Ann. Phys. **326**, 96 (2011).
[39] J. A. Kjäll, M. P. Zaletel, R. S. K. Mong, J. H. Bardarson, and F. Pollmann, Phys. Rev. B **87**, 235106 (2013).
[40] L. Seabra and F. Pollmann, Phys. Rev. B **88**, 125103 (2013).
[41] D. Sticlet, L. Seabra, F. Pollmann, and J. Cayssol, Phys. Rev. B **89**, 115430 (2014).
[42] A. A. Ovchinnikov, Zh. Eksp. Teor. Fiz. **57**, 2137 (1969) [Sov. Phys. JETP **30**, 1160 (1970)]; C. F. Coll, Phys. Rev. B **9**, 2150 (1974); F. Woynarovich, J. Phys. C **15**, 85 (1982); **15**, 97 (1982); **16**, 5293 (1983); J. M. P. Carmelo, P. Horsch, P. A. Bares, and A. A. Ovchinnikov, Phys. Rev. B **44**, 9967 (1991); F. H. L. Essler and V. E. Korepin, Nucl. Phys. B **426**, 505 (1994); T. Deguchi, F. H. L. Essler, F. Göhmann, V. E. Korepin, A. Klümper, and K. Kusakabe, Phys. Rep. **331**, 197 (2000).
[43] F. H. L. Essler and A. M. Tsvelik, Phys. Rev. B **57**, 10592 (1998); F. H. L. Essler and R. M. Konik, in *From Fields to Strings: Circumnavigating Theoretical Physics*, edited by M. Shifman, A. Vainshtein, and J. Wheater (World Scientific, Singapore, 2005) and references therein; arXiv:cond-mat/0412421.
[44] A. Shashi, L. I. Glazman, J.-S. Caux, and A. Imambekov, Phys. Rev. B **84**, 045408 (2011); A. Shashi and M. Panfil, J.-S. Caux, and A. Imambekov, *ibid.* **85**, 155136 (2012).
[45] P. Calabrese, F. H. L. Essler, and A. Läuchli, J. Stat. Mech. (2014) P09025.